

HALO FORMATION IN HIGH-INTENSITY LINACS: MODELING AND ADVANCED PHASE SPACE DIAGNOSTICS*

T. E. Thompson[†], A. Aleksandrov, K. Ruisard, A. Zhukov, ORNL, Oak Ridge, TN, USA

Abstract

Work at the Spallation Neutron Source (SNS) Beam Test Facility (BTF) aims to characterize halo formation in the early stages of a high-power linac and to reproduce halo measurements using well-benchmarked particle-in-cell simulations. The BTF is equipped with advanced phase space diagnostics that enable detailed characterization of beam distributions at the beginning and end of a 2.5 MeV, 10-meter test beamline. Diagnostic capabilities include direct measurement of the 6D phase space distribution, as well as imaging of 2D phase space projections with 6 orders of magnitude in dynamic range. This talk compares predictions from the PyORBIT code to measured distributions and discusses the parameters and limitations of the simulation model.

INTRODUCTION

The Beam Test Facility (BTF) is a Front-End replica of the Spallation Neutron Source (SNS), using an identical ion source and radio frequency quadrupole (RFQ) to produce a medium energy (2.5 MeV) H- beam. Downstream of the RFQ is a diagnostic heavy ~10-meter beam line with the capability to perform 6D measurements [1] and 2D high dynamic range (HDR) measurements [2, 3]. In addition to these diagnostics, the BTF contains a 9.5 cell permanent magnet quadrupole FODO line, allowing for beam transport studies [4] and the transport of matched and mismatched beams.

During initial conditioning, the SNS's optics settings were configured for the designed matched case but had higher-than-acceptable loss levels [5]. To get to its current loss level, the optics are continually empirically adjusted driving the SNS from a matched condition to a mismatched one. One source of losses in the SNS is the formation of halo, potentially driven by mismatch. Understanding the relationship between halo and mismatch provides insight into the SNS loss mechanisms and the reasons behind the SNS operating in a mismatched optics condition. The novel HDR measure-

ments at the BTF allow for scans that measure the beam distribution from the beam's high-density core to regions at 10^{-6} of peak particle density (approximate loss tolerance to meet <1 W/m losses for a 1 GeV H- beam).

This research aims to explore the effect of mismatch on the expansion of emittance and formation of halo in a medium energy beam. It aims to expand the groundwork laid by the Low Energy Demonstration Accelerator (LEDA) at Los Alamos National Lab (LANL) [6] by increasing the dynamic range of phase space measurements to 10^6 with novel HDR measurement capabilities significantly improving upon previous phase space diagnostics [3].

DEFINING MATCH, MISMATCH, AND HALO

This research uses the following definitions for match, mismatch and halo:

Match:

- The phase space that produces the lowest maximal RMS amplitude in the FODO line.

Mismatch:

- All phase spaces other than the matched phase space.
- Degree of mismatch determined with the Mismatch Factor (M) defined by:

$$M = \left[1 + \frac{\Delta + \sqrt{\Delta(\Delta + 4)}}{2} \right]^{1/2} - 1 \quad (1)$$

$$\Delta = (\Delta\alpha)^2 - \Delta\beta\Delta\gamma \quad (2)$$

$$\Delta\beta = \beta - \beta_m, \quad \Delta\alpha = \alpha - \alpha_m, \quad \Delta\gamma = \gamma - \gamma_m, \quad (3)$$

- Where the subscript m denotes the Twiss Parameters of the matched phase space.

Halo:

- All beam occupying regions of particle density below 10^{-4} of peak particle density.

DETERMINING MISMATCHED OPTICS CASES

All optics cases are defined by their Twiss Parameters a quarter-cell before the first FODO quad. There is only one matched case but a large region of possible mismatched cases. To narrow this region, this research considers only symmetric cases of mismatch where $\alpha_y = -\alpha_x$ and $\beta_y = \beta_x$.

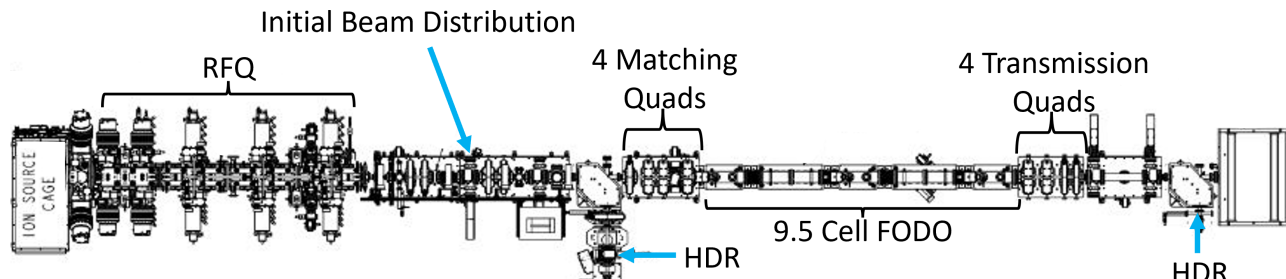


Figure 1: Layout of BTF. Initial beam distributions are measured with the first HDR diagnostics. The matching quads are used to manipulate the beams phase space before entering the FODO line, while the transmission quads are optimized for beam transmission. The output beam distributions are measured with the final HDR diagnostics.

Using this condition, all optics cases are discussed in terms of their x -plane Twiss Parameters.

To identify mismatch cases with high transmission, the FODO line was evaluated in simulation using Gaussian bunches. These bunches were generated with various transverse Twiss Parameters and emittances/longitudinal Twiss Parameters equivalent to measured distributions. After simulation through the FODO line, cases yielding high transmission defined a viable region of mismatch configurations. From this region, four specific Twiss Parameter sets were selected and define the cases analyzed. The region of high transmission and the cases chosen for analysis can be seen in Fig. 2. The Twiss Parameter values of these cases are detailed in Table 1. Each case will referred to by name in the "Optics Case" column.

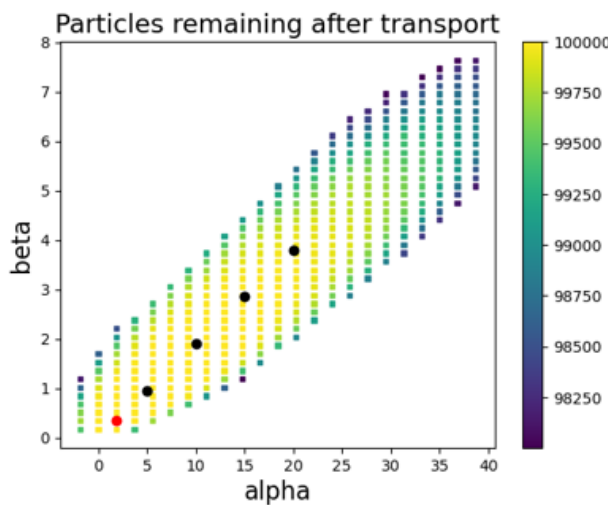


Figure 2: Particles remaining of simulated gaussian bunches transported through BTF FODO line. Red circle is location of matched condition. Black circles are the locations of the chosen mismatched cases.

Four quadrupoles before the FODO line (Matching Quads) were optimized in PyORBIT simulations to shape the beam core to the chosen Twiss Parameters in order to realize these phase spaces in the beam line [7]. Similarly, the four

quadrupoles after the FODO line (Transmission Quads) were optimized to maximize beam line transmission. Once magnet strengths were determined for each case, they were input in the physical beam line. However, these initial settings did not yield optimal transmission requiring further empirical optimization. Each case required adjustment of six steering correctors and the transmission quadrupoles to maximize transmission.

Table 1: Twiss Parameters and Mismatch Factors of the Matched Case and the Four Selected Mismatched Cases

Optics Case	Alpha	Beta	M	Trans.
Matched	1.837	0.339	0	95%
M 0.67	5.0	0.944	0.6677	94%
M 1.37	10.0	1.895	1.3639	93%
M 1.90	15.0	2.86	1.9046	90%
M 2.35	20.0	3.796	2.346	86%

TAKING HIGH DYNAMIC RANGE MEASUREMENTS

The full procedure for performing High Dynamic Range (HDR) measurements is outlined in [3] with a shortened version provided here. The HDR measurements work by scanning the phase space with two drift separated slits that are independently controlled with read-back resolution of 0.02 mm against the .2mm slit width. Selected phase space beamlets then travel through a dipole to clear any electrons, protons, or hydrogen atoms from the beamlet that were created by H- particles scattering off the edges of the slits. A photo luminescent screen intercepts the beamlet and a pair of cameras collects the light emitted by the screen. To achieve 10^6 dynamic range the cameras are set up with one camera having high sensitivity which becomes saturated after the low-sensitivity camera begins to pick up signal above background. The sensitivity relationship has a linear gain factor between the cameras so the measured intensities can be stitched together forming a single measurement with 10^6 dynamic range.

Having designed, implemented, and optimized the optics cases, HDR measurements of the transverse planes are taken

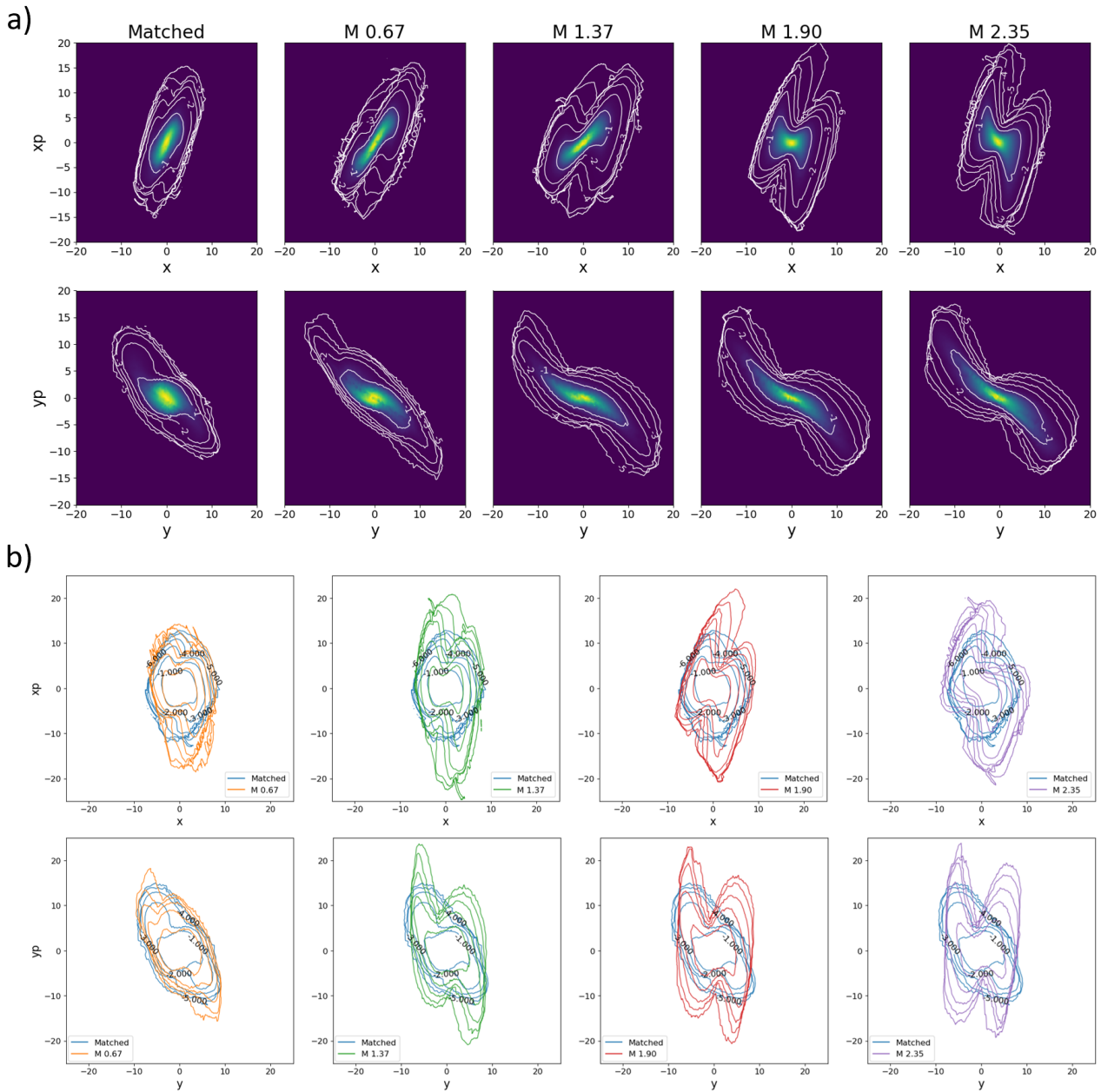


Figure 3: a): HDR measurements at end of beamline of various optics cases with increasing mismatch from left to right. Phase spaces are plotted in linear scale with log contours. Top: x,x' phase spaces. Bottom: y,y' phase spaces. b): Comparison of normalized phase spaces. Blue phase space in each plot is the matched case, other colors represent different mismatched cases. Top: x,x' phase spaces. Bottom: y,y' phase spaces.

for each case (Fig. 3). In some of the phase spaces there are straight line edges that are caused by scraping in the beamline. Though these edges are only evident in some cases, all cases have scraping. The scraping has different effects on the phase spaces due to the different optics of each case and the possibility of varying scraping locations. The matched, M 0.67 and M 1.37 cases have transmission of around 94% while transmission drops to 90% and 86% respectively for the two most mismatched cases M 1.90 and M 2.35.

NORMALIZING PHASE SPACES

To improve the visualization of halo in each of the optics cases the phase spaces are normalized by taking the Twiss Parameters of the 90% contour and applying the standard normalization transformation:

$$x_n = \sqrt{\frac{1}{\beta}} \cdot x \quad (4)$$

$$x'_n = \frac{\alpha}{\sqrt{\beta}} \cdot x + \sqrt{\beta} \cdot x' \quad (5)$$

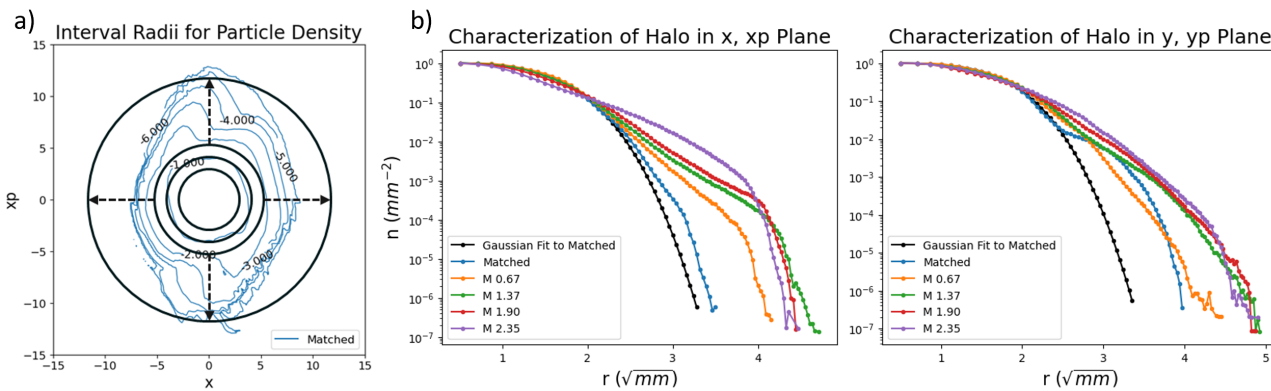


Figure 4: a): Example of the interval radii used to discretize normalized phase spaces. Particle numbers are counted in each dr ring. b): Phase space densities of matched and mismatched cases. In black is a Gaussian fit to the matched case.

A direct comparison of the mismatch cases to the matched case shows the increased width of the low density contours better after the phase spaces are normalized (Fig. 3). The low density contours increase in width and particle population as mismatch increases from left to right. This trend is most evident in comparing the two plot sets on the far left and appears to stall moving farther right. This stalling is currently attributed to the increase in scraping in the halo region cutting off the expansion of the low density contours. Phase space density plots are created in order to more qualitatively compare halo and better visualize the effect of scraping.

PHASE SPACE DENSITIES

Phase space density plots convert 2D phase spaces into a 1D particle density plot that improves the qualitative comparison of halo between cases. To create the 1D particle density plots, the particle density of the normalized phase spaces is discretized and plotted by:

1. Calculate $r = \sqrt{x_n^2 + x_n'^2}$
2. Count the number of particles dN_r within dr intervals
3. Calculate normalized particle numbers $n(r) = \frac{dN_r}{\text{Area}}$
4. Plot $n(r)$ in log scale vs. r

The process is detailed and the outputs shown in Fig. 4. It is evident in these plots that all cases have an increased particle population in low density regions than what a Gaussian function would approximate. At larger mismatch, the expansion in particle density far from the core increases until scraping cuts it off. The scraping in each case is most evident in the x, x' phase density plots with the knee in the graphs at large r . Future efforts will focus on reducing this scraping in order to allow a full comparison between cases in low density regions.

BENCHMARK OF PYORBIT SIMULATION

The particle-in-cell (PIC) code PyORBIT is used to simulate the BTF [7]. As a PIC code, PyORBIT takes in a set of

macroparticle phase space coordinates that approximate the particle distribution and transports it along a virtual beam line defined by a lattice file. The model includes:

1. Soft edged quadrupole magnet model
2. Quadrupole field strengths calibrated by direct measurement
3. Ideal quadrupole fields (no higher order terms)
4. Space charge by 3D FFT solver
5. Space charge potential from identical neighboring bunches

The upstream diagnostics in the BTF allow for bunches to be created from direct measurement. To create these bunches three 2D measurements in $x, x', y, y',$ and z, z' are sampled to approximate a 6D bunch.

The initial bunch for all five cases is identical and created in simulation from a set of low dynamic range 2d phase space measurements of the beam 1.3 m downstream of the RFQ. This is due to all cases having near identical optics before the matching quadrupoles with the only difference being slightly different corrector dipole strengths. As the bunch is transversely centered in simulation and these corrector differences are not currently implemented in the benchmark model, the simulation for each case then only differs in the magnet strengths for the matching and transmission quadrupoles. Once each case is simulated, the phase spaces are compared against measurement.

The benchmark comparison is shown in un-normalized phase space in Fig. 5. This figure makes it evident that current simulations are able to accurately predict the core of the beam for the matched condition. However, simulation accuracy gradually decreases as mismatch increases until, at the highest mismatch, even the inner most contours (representing 50% of the measured beam current) do not align.

The goal of ongoing studies is to validate the PyORBIT PIC model to the one part-per-million level, far below the

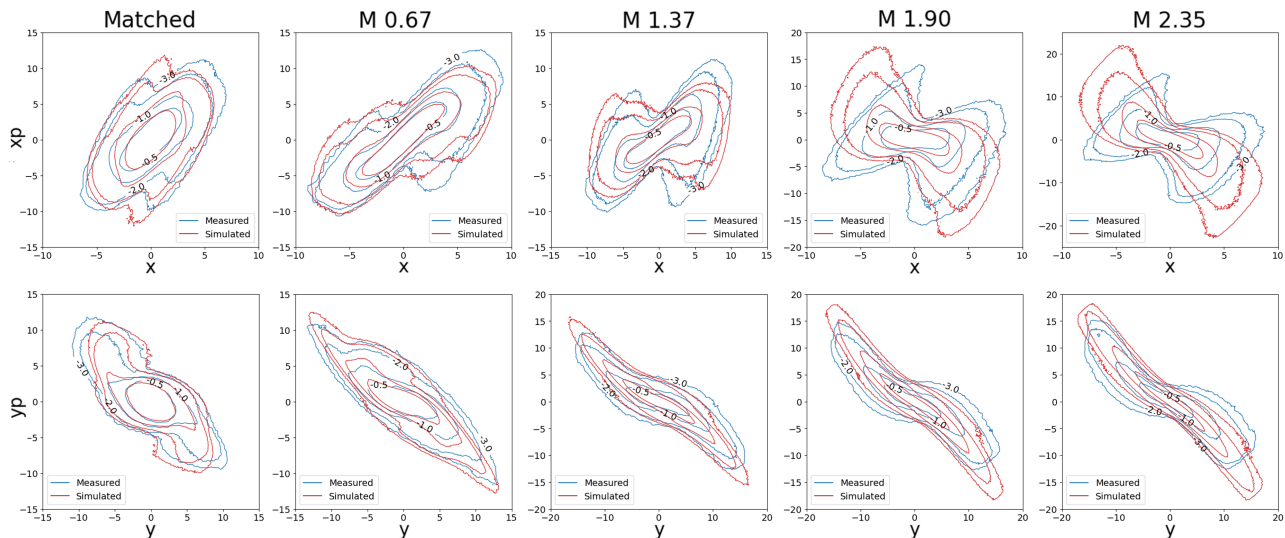


Figure 5: Comparison between Simulation and Measurement in Un-Normalized Phase Space with mismatch increasing from left to right. Top: x,x' phase spaces. Bottom: y,y' phase spaces.

discrepancy shown in Fig. 5. Uncorrected beam trajectory is one effect that will limit simulation accuracy. Bunches in the BTF are not centered which the simulation does not account for. While PyORBIT has the ability to simulate off-centered bunches, the diagnostic capability of the BTF is limited. This leads to scraping that cannot be reproduced by a simulation with a centered bunch. Efforts have been made to systematically explore possible off-center bunch parameters in simulation to reproduce observed scraping, however this is computationally expensive and has not led to better agreement.

We are in the process of determining optimal locations for additional correctors in order to improve beam steering because the current six correctors are not sufficient to center the bunch along the length of the BTF. We are confident that this is a steering issue and not an alignment issue as the BTF has been recently surveyed and components have positional tolerances of 0.2 mm.

In addition to addressing the steering issue other paths to improving simulation accuracy are being explored. This includes: adding higher order magnetic field terms and beam-based calibrations of quadrupole strengths.

CONCLUSION AND WHAT'S NEXT

Continuous high dynamic range measurements from the core to regions at 10^{-6} of peak particle density have been performed at various levels of mismatch. By analyzing these measurements using phase space density plots it is evident that particle density far from the core increases with larger mismatch. However, significant scraping complicated interpretation of these results.

Benchmarking of the BTF to simulation have produced accurate results in the core of matched and low mismatch beams. However, as mismatch increases simulation accuracy decreases and in the highest mismatch cases the inner most

contours fail to agree. Improvements to the BTF beamline and the PyORBIT simulation are under way to improve benchmarking capabilities.

To further investigate the relationship between halo and mismatch, the 5 optics cases presented here will be further optimized and transmission improved with additional correctors. By reducing scraping, measurement of halo in high mismatch cases will be possible. Additional optics cases will be explored outside of the restricted symmetric mismatch cases, including determining the feasibility of launching pure mismatch modes.

REFERENCES

- [1] B. Cathey, S. Cousineau, A. Aleksandrov, and A. Zhukov, “First Six Dimensional Phase Space Measurement of an Accelerator Beam”, *Phys. Rev. Lett.*, vol. 121, pp. 064804, 2018. doi: 10.1103/PhysRevLett.121.064804
- [2] K. Ruisard, A. Aleksandrov, S. Cousineau, A. Sishlo, and A. Zhukov, “Beyond RMS: Understanding the Evolution of Beam Distribution in High Intensity Linacs”, in *Proc. IPAC’21*, Campinas, Brazil, May 2021, pp. 3681-3685. doi: 10.18429/JACoW-IPAC2021-THXA01
- [3] A. Aleksandrov, S. Cousineau, K. Ruisard, and A. Zhukov, “First Measurement of a 2.5 MeV RFQ output emittance with 1 part-per-million dynamic range”, *Nucl. Instrum. Methods Phys. Res., Sect. A*, vol. 987, p. 164829, 2021. doi: 10.1016/j.nima.2020.164829
- [4] T. E. Thompson, A. Aleksandrov, T. Gorlov, K. Ruisard, and A. Shishlo, “Effect of Three-Dimensional Quadrupole Magnet Model on Beam Dynamics in the FODO Line at the Spallation Neutron Source Beam Test Facility”, in *Proc. HB’23*, Geneva, Switzerland, Oct. 2023, pp. 65-67. doi: 10.18429/JACoW-HB2023-TUC1C1
- [5] A. Shishlo, J. Galambos, A. Aleksandrov, V. Lebedev, and M. Plum, “First Observation of Intrabeam Stripping of Negative Hydrogen in a Superconducting Linear Accelerator”, *Phys.*

Rev. Lett., vol. 108, p. 114801, 2012.

doi:10.1103/PhysRevLett.108.114801

- [6] J. Qiang, P. L. Colestock, D. Gilpatrick, H. V. Smith, T. P. Wangler, and M. E. Schulze, “Macroparticle Simulation Studies of a Proton Beam Halo Experiment”, in *Phys. Rev. ST Accel. Beams*, vol. 5, p. 124201, 2002.
doi:10.1103/PhysRevSTAB.5.124201

- [7] A. Shishlo, S. M. Cousineau, J. Holmes, and T. Gorlov, “The Particle Accelerator Simulation Code PyORBIT”, *Procedia Comput. Sci.*, vol. 5, pp. 1272–1281, 2015.
doi:10.1016/j.procs.2015.05.312